Bio-inspired passive actuator simulating an abalone shell mechanism for structural control

2010 Smart Mater. Struct. 19 105011

(http://iopscience.iop.org/0964-1726/19/10/105011)

Smart Mater. Struct. **19** (2010) 105011 (11pp) doi:10.1088/0964-1726/19/10/105011

Bio-inspired passive actuator simulating an abalone shell mechanism for structural control

Henry T Y Yang[1], Chun-Hung Lin[1,3], Daniel Bridges[2], Connor J Randall[2] and Paul K Hansma[2]

[1] Department of Mechanical Engineering, University of California, Santa Barbara, CA 93106, USA
[2] Department of Physics, University of California, Santa Barbara, CA 93106, USA

E-mail: lin@engineering.ucsb.edu

Received 8 April 2010, in final form 2 July 2010
Published 6 August 2010
Online at stacks.iop.org/SMS/19/105011

Abstract
An energy dispersion mechanism called 'sacrificial bonds and hidden length', which is found in some biological systems, such as abalone shells and bones, is the inspiration for new strategies for structural control. Sacrificial bonds and hidden length can substantially increase the stiffness and enhance energy dissipation in the constituent molecules of abalone shells and bone. Having been inspired by the usefulness and effectiveness of such a mechanism, which has evolved over millions of years and countless cycles of evolutions, the authors employ the conceptual underpinnings of this mechanism to develop a bio-inspired passive actuator. This paper presents a fundamental method for optimally designing such bio-inspired passive actuators for structural control. To optimize the bio-inspired passive actuator, a simple method utilizing the force–displacement–velocity (FDV) plots based on LQR control is proposed. A linear regression approach is adopted in this research to find the initial values of the desired parameters for the bio-inspired passive actuator. The illustrative examples, conducted by numerical simulation with experimental validation, suggest that the bio-inspired passive actuator based on sacrificial bonds and hidden length may be comparable in performance to state-of-the-art semi-active actuators.

(Some figures in this article are in colour only in the electronic version)

1. Introduction

Abalone shell is 3000 times more fracture resistant than crystalline calcium carbonate, even though it is composed of 97% crystalline calcium carbonate (Jackson *et al* 1988). Part of the secret is the amazing mechanical performance of the other 3%, which is organic, primarily proteins (Smith *et al* 1999), working together with the structural geometry (Evans *et al* 2001, Schaffer *et al* 1997, Fritz *et al* 1994, Zaremba *et al* 1996). In bone, a small percentage by weight of non-collagenous proteins, such as osteopontin, contributes significantly to the fracture resistance (Thompson *et al* 2001, Hansma *et al* 2005, Fantner *et al* 2006b, 2007).

The key points in both abalone shells and bones are: (1) the work that must be done against entropy to stretch the hidden length is of an order 30 times greater than the work to break these strong bonds, and (2) the sacrificial bonds can reform, thus the work done against entropy is non-destructive (Thurner *et al* 2006, 2007). The goal of this research is to find new ways to dissipate energy generated by threats such as earthquakes, winds, impacts, or even blasts to civil and mechanical infrastructures, flutter of aircraft wings, bridges, cooling towers, and more.

What can be learned from abalone shell and bone that could help move the field of structural control forward? One lesson that can be learned is how to develop bio-inspired passive actuators. Both abalone shells and bones have distributed passive actuators that use the mechanism

[3] Author to whom any correspondence should be addressed.

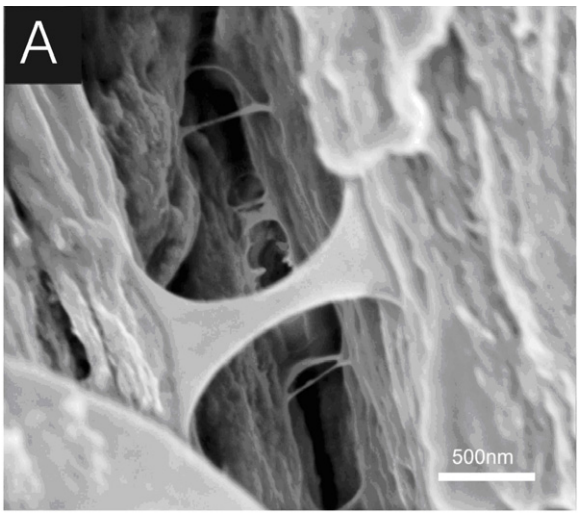

Figure 1. The molecules with sacrificial bonds and hidden length in the scanning electron microscope image of bone being fractured (Smith *et al* 1999, Fantner *et al* 2005, 2006a).

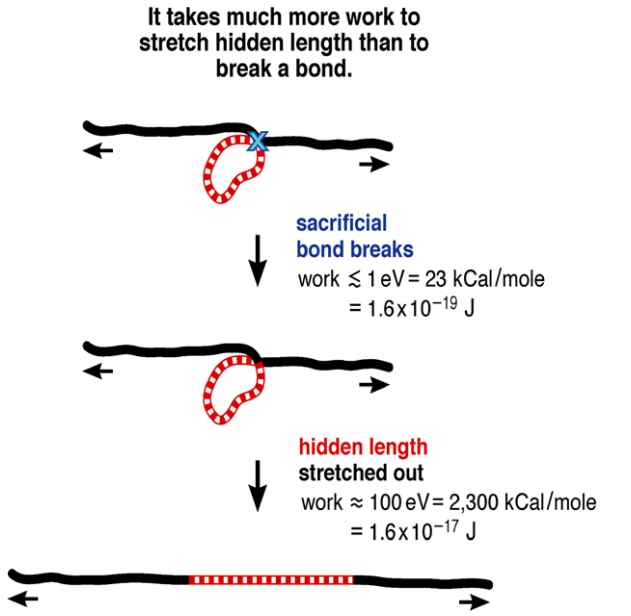

Figure 2. Schematic drawing of the sacrificial bond–hidden length mechanism (Fantner *et al* 2006a).

of sacrificial bonds and hidden length. Figure 1 shows a scanning electron microscope image of bone being fractured; the molecules with sacrificial bonds and hidden length can be seen resisting the start of the fracture (Smith *et al* 1999, Fantner *et al* 2005, 2006a). The biological system with sacrificial bonds and hidden length mechanism can dissipate energy from threats. A schematic drawing of the basic principle of the sacrificial bond and hidden length mechanism is shown in figure 2. Before the sacrificial bond is broken, only the solid length of the molecule contributes to the entropic spring (Kuhn and Grun 1942, Kratky and Porod 1949) and therefore to the force with which the molecule resists the stretching. The dotted length of the molecule is hidden from the applied force by the sacrificial bond. When the bond breaking force is reached, only a small amount of energy is required to break the sacrificial bond. After that, the whole length (solid plus dotted) contributes to the entropy of the molecule. This mechanism is very different from the mechanisms of dashpots and springs used in conventional engineered actuators.

In abalone shells, bone, and titin (found in muscle), there are many sacrificial bonds in each molecule and many molecules acting in series and parallel. The many sacrificial bonds in each molecule give a 'sawtooth' appearance to force versus displacement plots (figure 3). The basic sacrificial bond/hidden length mechanism appears in many other biological systems, including diatoms (Gebeshuber *et al* 2003), spider silk (Becker *et al* 2003), tendons (Gutsmann *et al* 2005), mussels (Hassenkam *et al* 2004), and the glue that sand-castle worms use to adhere grains of sand (Sun *et al* 2007). The mechanism has also been suggested for fabricating synthetic lightweight, damage resistant nanocomposite materials (Hansma *et al* 2007). Inspired by the concepts employed by the sacrificial bond–hidden length mechanism, this paper presents the optimal design of a passive actuator for structural control. Illustrative examples are presented to demonstrate the efficacy of the proposed system; performance is compared with current active and semi-active actuators. The authors believe the utilization of biologically inspired energy dissipation mechanisms may provide an innovative idea toward a new generation of structural control technology.

In the field of structural control, significant efforts have been devoted to protect civil infrastructures using various control strategies and devices, including the passive and active structural control methods summarized by Soong and Costantinou (1994). Passive devices generally require no external energy source to serve their purpose, as opposed to active devices which need external energy to apply forces to a structure. Recently, Soong and Spencer (2002) have reviewed the state-of-the-art passive structural control systems, which generally operate on principles such as frictional sliding, yielding of metals, phase transformation in metals, deformation of viscoelastic (VE) solids or fluids, and fluid orificing. On the other hand, semi-active control devices, also known as hybrid devices, combine the best features of both passive and active devices, offering the reliability of the passive devices while retaining the versatility and adaptability of the active devices. A survey paper dealing with energy dissipation and different kinds of actuators is given by Housner *et al* (1997). Researchers have investigated the possibility of using active, hybrid, and semi-active control methods to improve upon passive approaches to reduce structural responses (Spencer Jr and Nagarajaiah 2003).

Various state-of-the-art semi-active devices have been proposed and developed for civil infrastructural applications. For example, Dyke *et al* (1996) and Spencer Jr *et al* (1997) have proposed the magnetorheological (MR) dampers for seismic response reduction. Scruggs and Iwan (2003) have proposed another semi-active electrical machine for civil structural control. Chen and Chen (2004) have designed and tested the semi-active piezoelectric friction dampers on a quarter-scale building model.

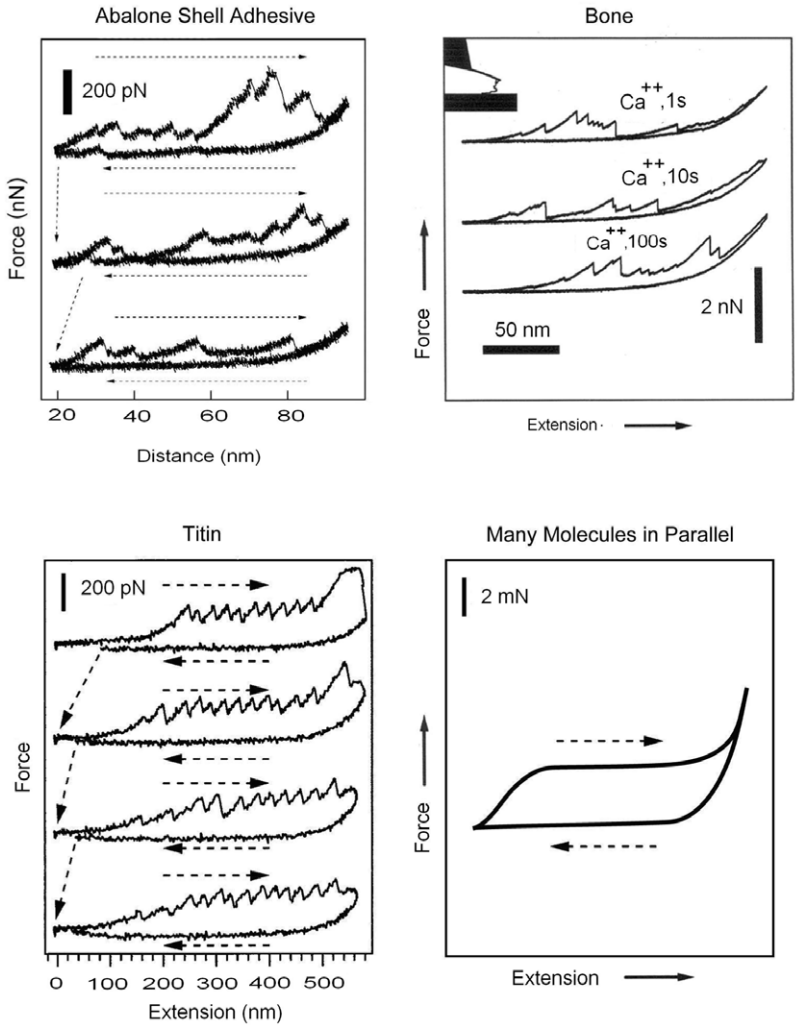

Figure 3. Force versus displacement plots for many different biological examples of the sacrificial bond–hidden length mechanism.

To illustrate and prove the concept of using the inspiration from sacrificial bonds and hidden length to design bio-inspired actuators for structural control applications, a model building structure subjected to seismic input is chosen as an example. The primary reason for using building response to earthquake excitation as the present model is because of the high level of work done in the field; it will be possible to compare the present results to the state-of-the-art examples which have already been developed. Additionally, structural models similar to those already constructed (Spencer Jr *et al* 1998) can be tailor built to experimentally test the usefulness and effectiveness of the bio-inspired passive actuators developed in this study.

In this research, the authors test the biologically inspired passive actuators using numerical simulation with experimental validation on a three-story model building similar to that proposed by Dyke *et al* (1996). The control performance of the proposed bio-inspired passive actuator is compared with well developed semi-active actuators using the same structural control example. The examples shown here demonstrate that the proposed bio-inspired passive control devices can achieve comparable performance to state-of-the-art semi-active devices.

2. Optimal passive actuator

The force versus displacement and velocity for the sacrificial bond–hidden length mechanism is very different from that of conventional passive actuators. A type of plot, the force–displacement–velocity plot (FDV plot), is presented in this study to facilitate the optimization of passive actuator systems to each structural system.

Considering a seismically excited structure with actuators on given floors, the equation of motion (Craig Jr 1981) can be written as

$$\mathbf{M}_s\ddot{x} + \mathbf{C}_s\dot{x} + \mathbf{K}_s x = \Gamma f - \mathbf{M}_s\Lambda\ddot{x}_g \tag{1}$$

where x is a vector of the displacements of each floor, $\ddot{x}_g$ is, for simplicity, a one-dimensional ground acceleration, f is the control force applied by the actuator installed on the structure, $\mathbf{\Gamma}$ and $\mathbf{\Lambda}$ are the location matrices, and $\mathbf{M}_s$, $\mathbf{C}_s$, and

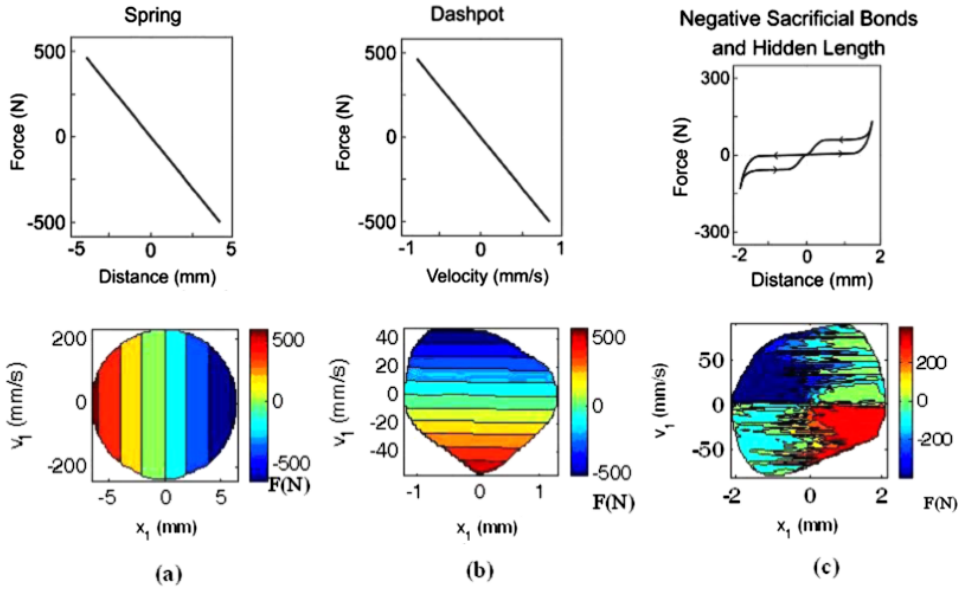

Figure 4. Force–displacement–velocity plots of three kinds of passive control forces at the first floor of the model considered by Dyke *et al* (1996) for 1,250 sets of values of displacement x_1 and velocity v_1 over the first 5 s, with $\Delta t = 0.004$ s, of N–S acceleration components of the scaled 1940 El Centro earthquake: (a) spring constant = 1000 (N cm^{-1}); (b) damping coefficient = 110 (N s cm^{-1}); (c) forces caused by the bio-inspired system with negative sacrificial bonds and hidden length.

$\mathbf{K}_s$ are the mass, damping and stiffness matrices of the linear system, respectively. Equation (1) can be written in state-space representation as

$$\dot{z} = \mathbf{A}z + \mathbf{B}f + \mathbf{E}\ddot{x}_g \tag{2}$$

where z is the state vector. The measurement equation is given by

$$y = \mathbf{C}z + \mathbf{D}f + v \tag{3}$$

where y is the vector of measured outputs, v is the noise vector in measurement, and $\mathbf{A}$, $\mathbf{B}$, $\mathbf{C}$, $\mathbf{D}$ and $\mathbf{E}$ are the state-space matrices, which are the same as those defined in Dyke *et al* (1996) and given by

$$\mathbf{A} = \begin{bmatrix} \mathbf{0} & \mathbf{I} \\ -\mathbf{M}_s^{-1}\mathbf{K}_s & -\mathbf{M}_s^{-1}\mathbf{C}_s \end{bmatrix} \qquad \mathbf{B} = \begin{bmatrix} \mathbf{0} \\ \mathbf{M}_s^{-1}\mathbf{\Gamma} \end{bmatrix} \qquad \mathbf{E} = -\begin{bmatrix} \mathbf{0} \\ \mathbf{\Lambda} \end{bmatrix} \tag{4}$$

and

$$\mathbf{C} = \begin{bmatrix} -\mathbf{M}_s^{-1}\mathbf{K}_s & -\mathbf{M}_s^{-1}\mathbf{C}_s \\ 1\,0\,0 & 0\,0\,0 \end{bmatrix} \qquad \mathbf{D} = \begin{bmatrix} \mathbf{M}_s^{-1}\mathbf{\Gamma} \\ \mathbf{0} \end{bmatrix}. \tag{5}$$

The force–displacement–velocity plot (FDV plot) presented here is a contour plot of the control force applied on a structure as a function of the displacement and velocity under a specific excitation. Figure 4 shows the simulating results of three kinds of passive control forces at the first floor of the three-story structural model considered by Dyke *et al* (1996) for the displacement (x_1) and velocity (v_1) over the first 5 s, while excited by the N–S acceleration components of the scaled 1940 El Centro earthquake. Figures 4(a) and (b) show a typical spring and a typical dashpot where the force is in the opposite direction of its displacement or velocity. Figure 4(c) shows a bio-inspired actuator based on the negative sacrificial bond and hidden length, which will be discussed in detail in section 3. It is noted that the force–displacement–velocity plot for the bio-inspired passive actuator based on sacrificial bonds and hidden length (figure 4(c)) is quite different from the force–displacement–velocity plots of the traditional type of damping systems of springs and dashpots. There are two basic variations to this type of bio-inspired actuator: the force which resists motion is greater either (1) as the structure moves away from the equilibrium position or (2) as the structure moves towards the equilibrium position. Figure 4(c) shows the second case, which is called 'negative' sacrificial bonds and hidden length. For example, when displacement from equilibrium, x_1, is positive, the force is greater for negative velocity than for positive velocity, v_1.

With the aid of force–displacement–velocity plots (FDV plots), the bio-inspired passive actuators in the structural model can be optimized. First, for example, the linear–quadratic regulator (LQR) optimization (Kwakernaak and Sivan 1972) is used to find the ideal or desired force–displacement–velocity plot (shown in figure 5) of an active actuator during a simulated earthquake. The objective of using a LQR optimization is to minimize a cost function of

$$J = \lim_{t\to\infty} \int_0^t (y^{\mathrm{T}}\mathbf{Q}y + f^{\mathrm{T}}\mathbf{R}f)\,\mathrm{d}t \tag{6}$$

where $\mathbf{Q}$ and $\mathbf{R}$ are the weighting matrices and can be changed due to the mechanical dynamics of the system under consideration.

Since actuators with similar FDV plots may have similar control performance, efforts are then made to replicate this FDV plot of an active actuator with a combination of

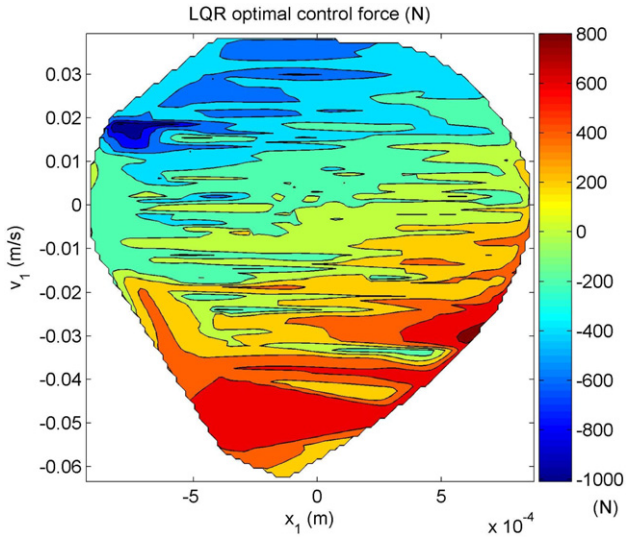

Figure 5. Force–displacement–velocity plots calculated on the model considered by Dyke *et al* (1996) over the N–S acceleration components of the scaled 1940 El Centro earthquake with LQR optimal control force. The LQR is based on the minimization of cost function: $J = \lim_{t\to\infty} \int_0^t (1.83 \times 10^6 \ddot{x}_3^2 + 7.2 \times 10^{12} x_1^2 + 1.0 f_1^2)\, \mathrm{d}t$.

components from the current bio-inspired pallet of passive actuators. By choosing the appropriate parameters of the bio-inspired passive actuator, it is possible to construct the optimal passive actuator to control the structure during a specific earthquake.

3. Design of bio-inspired actuator

For the three-story model structure considered by Dyke *et al* (1996), the force–displacement–velocity plot cannot be simulated using a linear combination of conventional dampers and springs. In fact what is needed is the addition of a component to tilt the force–displacement–velocity plot of a damper the opposite way from adding a conventional spring. From biology, the authors are inspired to evolve a device that will optimize force–displacement–velocity plot and hence optimize the control of structural vibrations. The simple mechanical model of the bio-inspired system is shown in figure 6, which formed the basis for the numerical simulation model and for the construction of the passive actuators used in this research. The applied force f predicted by the model is given by

$$f = \mathrm{BIO}(x, \dot{x}) + C_0 \dot{x} \tag{7}$$

where $\mathrm{BIO}(x, \dot{x})$ is the force generated by the bio-inspired mechanism, and C_0 is the damping coefficient.

In this study, the function $\mathrm{BIO}(x, \dot{x})$ is defined by

$$\mathrm{BIO}(x, \dot{x}) = \begin{cases} f_{\max} & \text{if } x \geqslant 0 \quad \text{and} \quad \dot{x} \leqslant 0 \\ -f_{\max} & \text{if } x \leqslant 0 \quad \text{and} \quad \dot{x} \geqslant 0 \\ 0 & \text{if } x \cdot \dot{x} > 0 \end{cases} \tag{8}$$

where $f_{\max}$ is the maximum force assumed in the sacrificial bond/hidden length mechanism.

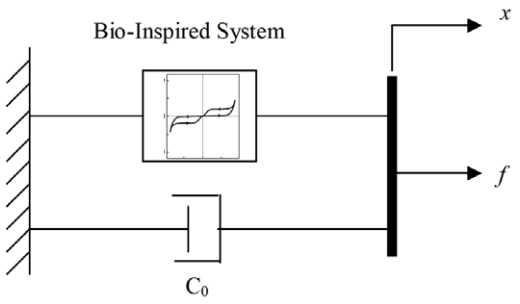

Figure 6. Simple mechanical model of the bio-inspired system as the basis for the numerical simulation and the construction of passive actuators.

A statistical approach is utilized in this study to determine the parameters of the optimal passive actuator. Since the force–displacement–velocity plot of the LQR control over a specific earthquake (figure 5) is desired, the linear regression is used to fit every point on the force–displacement–velocity plot:

$$F = \beta_{\text{spring}} \times x_1 + \beta_{\text{damping}} \times v_1 + \beta_{\text{bio}} \times \mathrm{BIO} \tag{9}$$

where F is the desired control force from LQR control, and x_1 and v_1 are the displacement and velocity of the controlled floor, respectively. BIO is the unit force generated by the bio-inspired mechanism based on the negative sacrificial bonds and hidden length (figure 4(c)) with $f_{\max} = 1$ N. The coefficients on the independent variables, x_1, v_1, and BIO, are β_{spring}, β_{damping}, and β_{bio}, respectively. The values of β_{spring} and β_{damping} are equivalent to the spring coefficient, K_0, and the damping coefficient, C_0, respectively. The value of β_{bio} is equivalent to $f_{\max}$ in the $\mathrm{BIO}(x, \dot{x})$ function. The spring coefficient in (9) is used to show the idea of negative spring, which is similar to the negative sacrificial bond/hidden length mechanism and is not included in figure 6. The optimal control parameters of the bio-inspired passive controller defined in (9) can be obtained by linearly regressing (9) to the ideal FDV plot (figure 5). These values can be used as the initial values when optimizing the parameters of the control device.

4. Illustrative examples

4.1. Evaluation of the effectiveness of the concept using the bio-inspired passive actuators by numerical example

In order to prove the concept and to demonstrate the applicability and performance of the proposed bio-inspired passive actuator, a three-story numerical structure model is considered in this study. The equation of motion of the structure is given in equation (1), where $x = [x_1 x_2 x_3]^{\mathrm{T}}$ is the vector of displacements of the three floors. Since the bio-inspired actuator is installed on the first floor, the variable x in (5) and (6) is equal to x_1. The system matrices are the same as those documented in Dyke *et al* (1996) and given by

$$\mathbf{M}_s = \begin{bmatrix} 98.3 & 0 & 0 \\ 0 & 98.3 & 0 \\ 0 & 0 & 98.3 \end{bmatrix} \text{kg}$$

Table 1. Performance of LQR optimal control with different cost functions.

$Q(3,3)$	a_3		1.70×10^6	$\mathbf{1.83 \times 10^6}$	1.91×10^6	2.40×10^6	3.20×10^6
$Q(4,4)$	x_1	Uncontrolled	7.50×10^{12}	$\mathbf{7.20 \times 10^{12}}$	7.00×10^{12}	6.00×10^{12}	5.00×10^{12}
$R(1,1)$	f		1.00×10^0	$\mathbf{1.00 \times 10^0}$	1.00×10^0	1.00×10^0	1.00×10^0
Displacement (cm)	x_1	0.549	0.092	**0.093**	0.094	0.096	0.105
	x_2	0.837	0.141	**0.139**	0.139	0.136	0.136
	x_3	0.973	0.195	**0.191**	0.189	0.176	0.163
Drift (cm)	d_1	0.549	0.092	**0.093**	0.094	0.096	0.105
	d_2	0.318	0.096	**0.093**	0.091	0.082	0.071
	d_3	0.203	0.066	**0.065**	0.064	0.058	0.051
Acceleration (cm s^{-2})	a_1	1039	454	**450**	448	462	499
	a_2	1096	509	**500**	495	466	433
	a_3	1480	649	**637**	630	591	545
Max force (N)	f	0	941	**941**	941	941	941

Table 2. Regression of force–displacement–velocity plot using damping and bio-inspired force.

Regression statistics	
Multiple R	0.9018
R square	0.8133
Adjusted R square	0.8126
Standard error	155.63
Observations	1707

	Coefficients	Standard error	t stat	P-value	Lower 95%	Upper 95%
Intercept	0					
β_{damping} (N s m^{-1})	10 449.11	176.54	59.19	0	10 102.85	10 795.37
β_{bio} (N)	133.81	6.45	20.76	1.66×10^{-85}	121.16	146.45

$$\mathbf{C}_s = \begin{bmatrix} 175 & -50 & 0 \\ -50 & 100 & -50 \\ 0 & -50 & 50 \end{bmatrix} \text{N s m}^{-1}$$

$$\mathbf{K}_s = 10^5 \begin{bmatrix} 12.0 & -6.84 & 0 \\ -6.84 & 13.7 & -6.84 \\ 0 & -6.84 & 6.84 \end{bmatrix} \text{N m}^{-1} \qquad \mathbf{\Gamma} = \begin{bmatrix} 1 \\ 0 \\ 0 \end{bmatrix}$$

$$\mathbf{\Lambda} = \begin{bmatrix} 1 \\ 1 \\ 1 \end{bmatrix}.$$

To account for the model scale and to compare with the simulating results by Dyke *et al* (1996), the N–S acceleration components of the 1940 El Centro earthquake is timescaled by a factor of five and used as the excitation to the structure model in the proposed simulation. Due to the passive nature of the proposed bio-inspired actuator, there is no need to design a control strategy such as those usually used by active or semi-active control devices. In this example, the cost function of the LQR control is chosen in a way to minimize the third floor acceleration, the first floor displacement, and the applied control force. The cost function then is defined by

$$\begin{aligned} J &= \lim_{t\to\infty} \int_0^t (y^{\mathrm{T}}\mathbf{Q}y + f^{\mathrm{T}}\mathbf{R}f)\,\mathrm{d}t \\ &= \lim_{t\to\infty} \int_0^t (Q(3,3)\ddot{x}_3^2 + Q(4,4)x_1^2 + R(1,1)f_1^2)\,\mathrm{d}t \end{aligned} \tag{10}$$

where $\ddot{x}_3$ is the acceleration measured on the third floor of the structure model, x_1 and f_1 are the displacement and control force on the first floor, respectively. A comparison of LQR control with different cost functions is shown in table 1. In this research, $Q(3,3)$, $Q(4,4)$, and $R(1,1)$ are chosen to be 1.83×10^6, 7.20×10^{12}, and 1.0, respectively, to minimize the largest floor-to-floor drift, while the maximum control force is set to be 941 N to be the same as in the work done by Dyke *et al* (1996). This choice is different from those chosen by Scruggs and Iwan (2003), which can also successfully reduce the structural response. However, the results of control performance are close to each other. The LQR optimal control force based on (10) is used to derive the parameters of the bio-inspired passive controller defined in (9).

For example, if only the combination of damping and negative sacrificial bond/hidden length mechanism are considered, the result of the regression shows the damping coefficient to be 104.5 N s cm^{-1} and the $f_{\max}$ of negative sacrificial bond–hidden length to be 133.8 N with an R-squared value of 0.81. These two coefficients are both significant at 95% confidence level (table 2).

If only the stiffness and damping coefficients are considered, the regression suggests a negative spring constant of -2139 N cm^{-1} and a damping coefficient of 126.1 N s cm^{-1}. The negative spring constant means the structure is too stiff and can be softened to reduce the structural response. The R-squared value of the regression is 0.83, and both coefficients are significant at 95% confidence level (table 3).

If all three variables are considered, the regression suggests a negative spring constant of -1795.5 N cm^{-1}, a damping coefficient of 120.6 N s cm^{-1}, and $f_{\max}$ of 34.8 N.

Table 3. Regression of force–displacement–velocity plot using spring and damping.

Regression statistics	
Multiple R	0.9130
R square	0.8335
Adjusted R square	0.8328
Standard error	146.98
Observations	1707

	Coefficients	Standard error	t stat	P-value	Lower 95%	Upper 95%
Intercept	0					
β_{spring} (N m^{-1})	−213 901	8144.81	−26.26	6.1×10^{-128}	−229 876	−197 926
β_{damping} (N)	12 605.63	140.47	89.74	0	12 330.12	12 881.15

Table 4. Regression of force–displacement–velocity plot using spring, damping and bio-inspired force.

Regression statistics	
Multiple R	0.9138
R Square	0.8350
Adjusted R square	0.8342
Standard error	146.38
Observations	1707

	Coefficients	Standard error	t stat	P-value	Lower 95%	Upper 95%
Intercept	0					
β_{spring} (N m^{-1})	−179 548	12 013.39	−14.95	1.49×10^{-47}	−203 111	−155 986
β_{damping} (N s m^{-1})	12 062.22	198.04	60.91	0	11 673.79	12 450.66
β_{bio} (N)	34.81	8.98	3.88	0.00 011	17.20	52.42

The R-squared value of the regression is 0.83. All coefficients are significant at 95% confidence level (table 4).

The statistical approach based on linear regression can provide a good estimation of the parameters of the passive actuator. A better control performance can be achieved by tuning the parameters starting from the estimated values.

In this study, the value of C_0 and $f_{\max}$ are optimized and chosen to be 70 (N s cm^{-1}) and 350 (N), respectively, to maximize the performance. The simulation comparison of the bio-inspired passive actuator to the MR damper proposed by Dyke *et al* (1996) due to a 2.5 Hz sinusoid excitation with an amplitude of 1.5 cm is shown in figure 7. The force–displacement–velocity plot of this passive actuator is then calculated and shown in figure 8. It is noticed that the force–velocity–displacement plot here is tilted in the same way as the force–displacement–velocity plot based on LQR optimal control force (figure 5).

The structural responses of the example are compared to those using the semi-active MR damper (Dyke *et al* 1996, Spencer Jr *et al* 1997) and both are shown in figure 9. Figure 10 indicates that the proposed bio-inspired passive actuator can achieve a similar level of performance in floor displacements and acceleration response as the semi-active MR damper.

In the illustrative example, it seems that bio-inspired passive actuator systems based on sacrificial bonds and hidden length coupled with dampers could yield results comparable in performance to the state-of-the-art semi-active actuators developed by widely referenced publications in the field (Dyke *et al* 1996, Scruggs and Iwan 2003, Spencer Jr *et al* 1997). Comparisons of the present results in peak responses of the model structure considered in (Dyke *et al* 1996) and (Scruggs and Iwan 2003) over the scaled N–S acceleration component of the 1940 El Centro earthquake are shown in table 5. The simulation of a brushless DC machine achieves a very low acceleration response due to its mechanical dynamics of a larger mass on the first floor.

4.2. Experimental validation of the numerical simulation method using a three-story aluminum model with bio-inspired passive actuators

During this research, a specific three-story model is built out of aluminum, as shown in figure 11. The first three natural frequencies calculated from the finite element model are 2.15 Hz, 6.79 Hz, and 10.59 Hz, respectively. The experimentally measured frequencies are 2.00 Hz, 6.37 Hz, and 10.16 Hz, respectively. Two types of passive actuators to be installed on the first floor of this model are designed, built, and tested using the N–S acceleration component of the 1940 El Centro earthquake as the excitation. The first device is a simple friction block that slides on the platform of the present test model building (friction force = 0.2 N). The second one is a 'negative spring' (spring constant = −4.3 N cm^{-1}) plus a damper (damping coefficient = 0.117 N s cm^{-1}) mounted on the test model building. The negative spring with damping prototype device uses a commercial airpot damper (the black cylinder) together with a novel element that uses three magnets. Two magnets on a linear slide are attracted to a stationary magnet that is held in the arched structure mounted on the base. Figure 12 shows a comparison between theoretical predictions and experimental measurements using force–displacement–velocity plots for the two sets of prototype device—friction damper and negative spring damper. The friction damper is

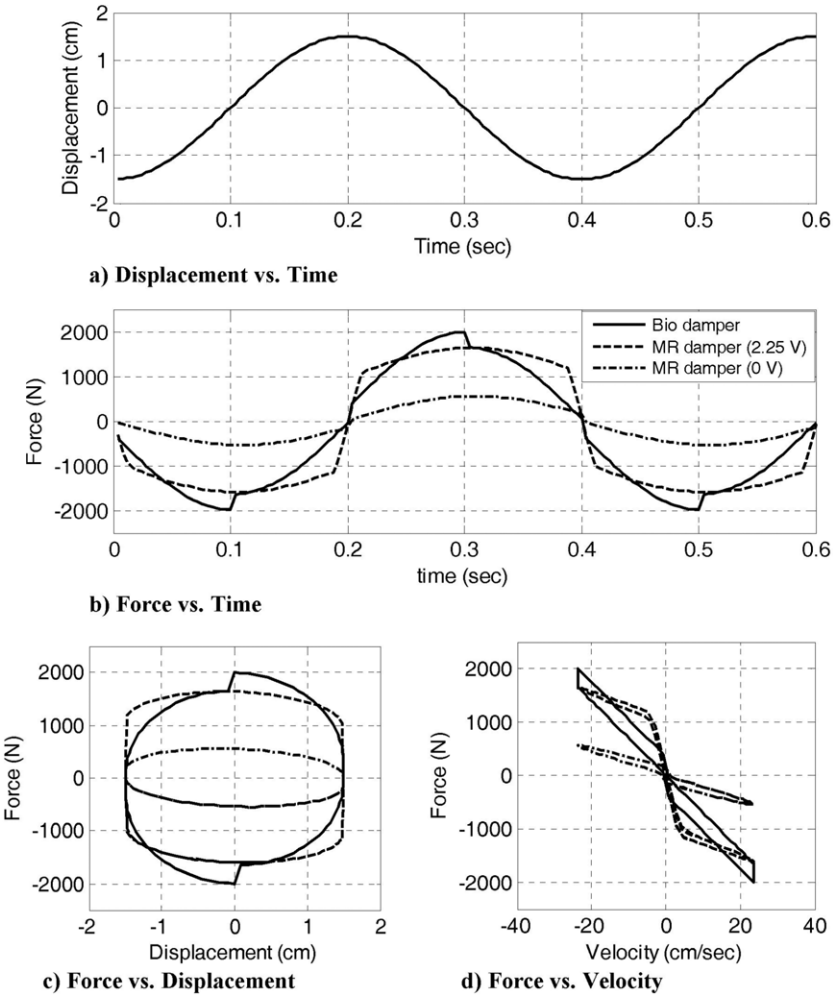

Figure 7. Simulation results of the bio-inspired passive actuator and MR damper for 2.5 Hz sinusoidal excitation with an amplitude of 1.5 cm.

Table 5. Comparisons of peak responses of displacements, drifts, and accelerations over the scaled 1940 El Centro earthquake using. (a) Active LQR control (bio-inspired active control based on bio-system with muscle, tendon and bone); (b) bio-inspired passive actuator based on bio-system with sacrificial bonds and hidden length; (c) semi-active magnetorheological (MR) damper (Dyke *et al* 1996); (d) semi-active brushless DC machine (Scruggs and Iwan 2003).

		Uncontrolled	Active LQR optimal control	Bio-inspired passive actuator (sacrificial bond and hidden length)					Semi-active MR damper	Semi-active BDC
			(a)	(b)					(c)	(d)
K_0 (N cm^{-1})				0	0	−2139	−1795.5	−1689		
C_0 (N s cm^{-1})				70	104.5	126	120.6	85		
f_{max} (N)				350	133.8	0	34.8	260		
Displacement (cm)	x_1	0.549	0.093	0.112	0.116	0.115	0.116	0.108	0.114	0.103
	x_2	0.837	0.139	0.169	0.195	0.163	0.165	0.149	0.185	0.152
	x_3	0.973	0.191	0.230	0.258	0.224	0.229	0.202	0.212	0.198
Drift (cm)	d_1	0.549	0.093	0.112	0.116	0.115	0.116	0.108	0.114	0.103
	d_2	0.318	0.093	0.092	0.106	0.101	0.100	0.090	0.090	0.088
	d_3	0.203	0.065	0.071	0.084	0.072	0.074	0.068	0.101	0.060
Acceleration (cm s^{-2})	a_1	1039	450	418	493	531	486	319	696	250
	a_2	1096	500	508	513	483	486	520	739	253
	a_3	1480	637	652	728	656	669	629	703	417
Max force (N)	f	0	941	754	702	698	705	763	941	749

employed here because it is a simple and common device. The negative spring damper has the desired property indicated in figure 5, and the proposed bio-inspired passive actuator is inspired by this kind of damper. Furthermore, the structural response of third floor displacement corresponding to the comparison in figure 12 is shown in figure 13. The agreements

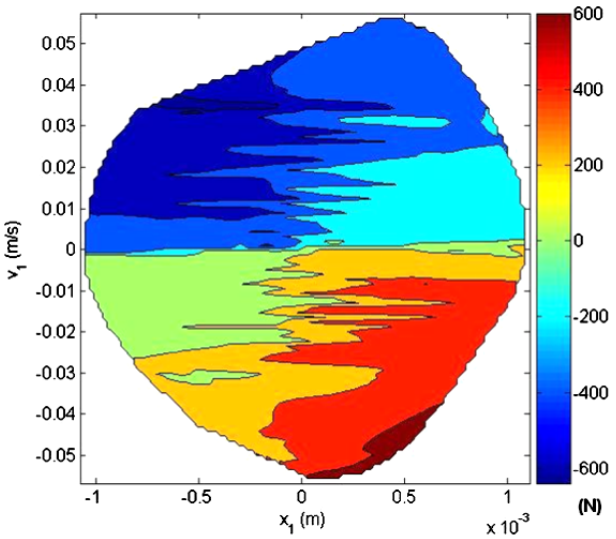

Figure 8. Force–displacement–velocity plots calculated on the model considered by Dyke *et al* (1996) over the N–S acceleration components of the scaled 1940 El Centro earthquake with bio-inspired passive actuator ($C_0 = 70$ N s cm^{-1} and $f_{\max} = 350$ N).

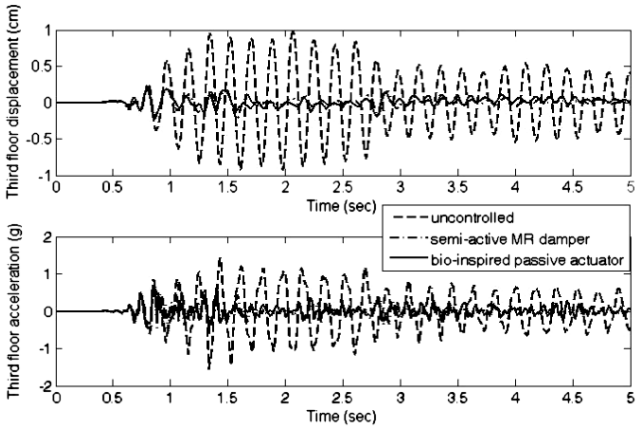

Figure 9. Uncontrolled structural responses as compared to these controlled by semi-active MR damper and bio-inspired passive actuator ($C_0 = 70$ N s cm^{-1} and $f_{\max} = 350$ N), respectively, due to the N–S acceleration component of the scaled 1940 El Centro earthquake.

in the two sets of the time-history displacement data for the first 10 s are convincing. Such comparison may indicate that reliable results can be obtained in the subsequent numerical simulations and validations of the presently suggested concept of bio-inspired passive actuator.

5. Conclusions

Inspired and challenged by the simplicity and enormous capability of actuators present in bio-organisms, the authors have successfully built passive actuators which compare favorably with state-of-the-art semi-active actuators, and with potential in the direction of bio-inspired research in the future. This paper presents a fundamental method of designing and optimizing bio-inspired passive actuators for structural control. The force–displacement–velocity plots based on LQR control and the statistic approach based on linear regression are adopted in this research.

Illustrative examples of two prototype passive dampers tested both theoretically and experimentally validate the development and also demonstrate the applications. The proposed bio-inspired actuators, although passive, are comparable in performance to state-of-the-art semi-active actuators in numerical simulations. It is noted that once the peak ground acceleration is changed, the situation will likely change. The accuracy of the control parameters used in numerical simulations, such as damping coefficient, spring constant, and $f_{\max}$ is important in order to predict the structural response more realistically. Besides, due to the simplicity

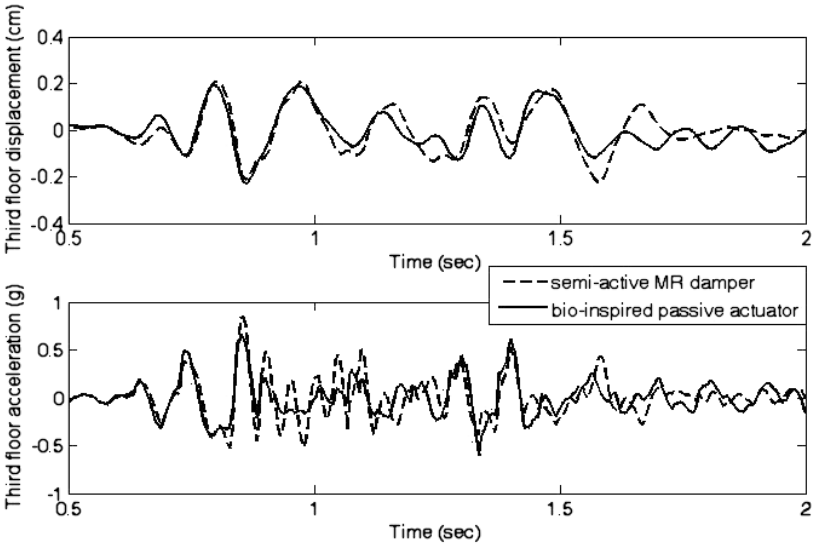

Figure 10. Detailed structural responses of those controlled by semi-active MR damper and bio-inspired passive actuator ($C_0 = 70$ N s cm^{-1} and $f_{\max} = 350$ N), respectively, due to the N–S acceleration component of the scaled 1940 El Centro earthquake.

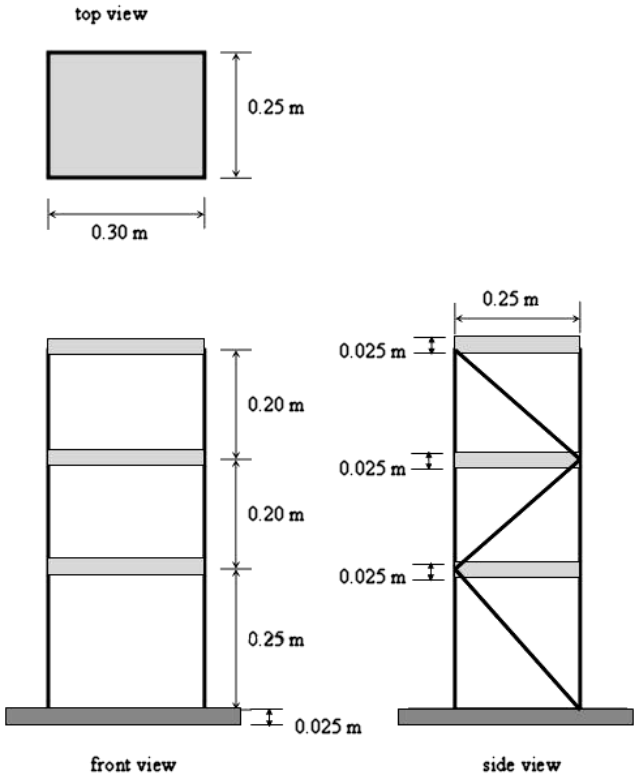

Figure 11. Three-story aluminum test model structure.

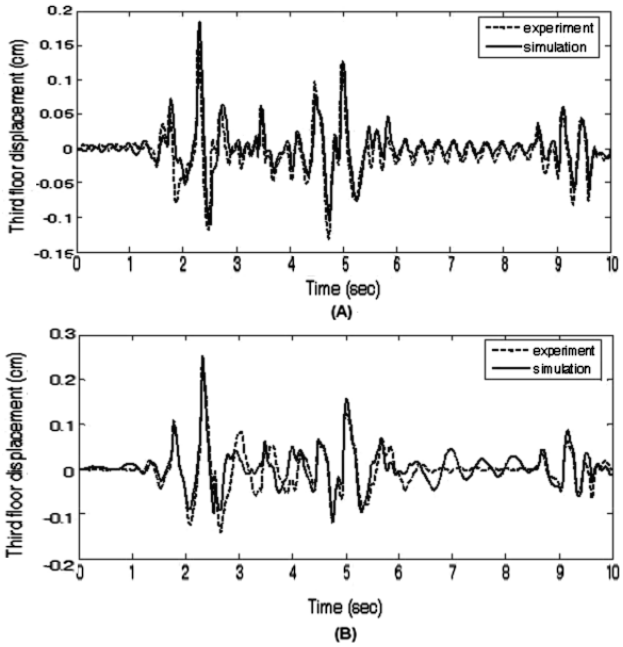

Figure 13. Third floor displacement of the present three-story aluminum test model building with the passive actuators: (A) friction damper; (B) negative spring with damping prototype device uses a commercial airpot damper.

of the bio-inspired actuator, the control devices are easy to design, and there is no need of any active control strategy. Furthermore, the control device is independent of inadvertent conditions such as power outage.

This research may have the potential to revitalize the field of structural protection with passive actuators. Biological structures, such as abalone shells and bone, have evolved over millions of years to make structures that are smart, resilient, efficient, and sustainable.

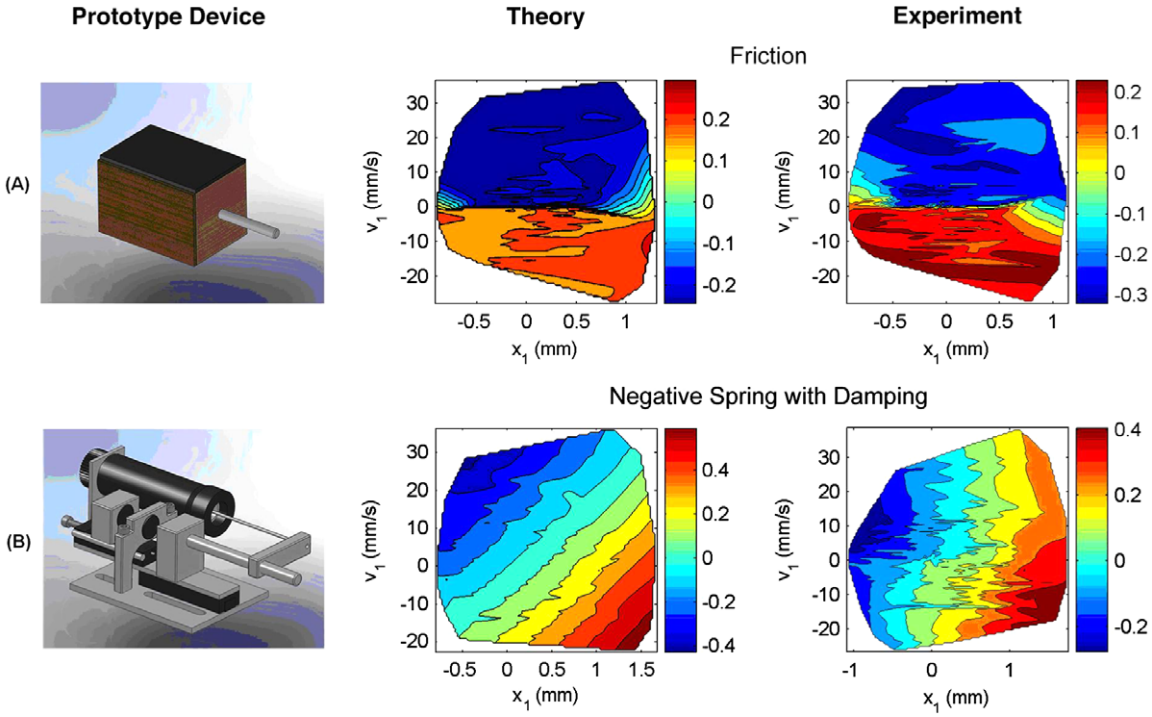

Figure 12. Passive actuators developed in this study and tested using the present experimental model structure with corresponding FDV plots: (A) friction damper; (B) negative spring with damping prototype device uses a commercial airpot damper.

This paper presents the concept of designing the passive actuator in a bio-inspired way. The desired force pattern can be achieved by specially designed devices, for example, the magnetic device is added as the negative spring in this research. The scale of applied force by the bio-inspired actuator in experiment is still a challenge. The remarkable mechanical properties due to the sacrificial bonds and hidden length mechanism found in abalone shells and bone will be investigated with more applications in the future. The bio-inspired actuators could be integrated into structures with health monitoring and control systems that are designed to mitigate damage from natural and human-made hazards.

Acknowledgments

This study is sponsored by the National Science Foundation grant CMS 0511046. The guidance of program director, Dr S C Liu, is gratefully acknowledged. The authors gratefully acknowledge the comments on their manuscript by Dr Bill Spencer.

References

Becker N, Oroudjev E, Mutz S, Cleveland J P, Hansma P K, Hayashi C Y, Makarov D E and Hansma H G 2003 Molecular nanosprings in spider capture-silk threads *Nat. Mater.* **2** 278–83

Chen C and Chen G 2004 Shake table tests of a quarter-scale three-storey building model with piezoelectric friction dampers *Struct. Control Health Monit.* **11** 239–57

Craig R R Jr 1981 *Structural Dynamics* (New York: Wiley)

Dyke S J, Spencer B F Jr, Sain M K and Carlson J D 1996 Modeling and control of magnetorheological dampers for seismic response reduction *Smart Mater. Struct.* **5** 565–75

Evans A G, Suo Z, Wang R Z, Aksay I A, He M Y and Hutchinson J W 2001 Model for the robust mechanical behavior of nacre *J. Mater. Res.* **16** 2475–84

Fantner G E, Adams J, Turner P, Thurner P J, Fisher L W and Hansma P K 2007 Nanoscale ion mediated networks in bone: osteopontin can repeatedly dissipate large amounts of energy *Nano Lett.* **7** 2491–8

Fantner G E *et al* 2005 Sacrificial bonds and hidden length dissipate energy as mineralized fibrils separate during bone fracture *Nat. Mater.* **4** 612–6

Fantner G E *et al* 2006a Sacrificial bonds and hidden length: unraveling molecular mesostructures in tough materials *Biophys. J.* **90** 1411–8

Fantner G E *et al* 2006b Hierarchical interconnections in the nano-composite material bone: fibrillar cross-links resist fracture on several length scales *Compos. Sci. Technol.* **66** 1205–11

Fritz M, Belcher A M, Radmacher M, Walters D A, Hansma P K, Stucky G D, Morse D E and Mann S 1994 Flat pearls from biofabrication of organized composites on inorganic substrates *Nature* **371** 49–51

Gebeshuber I C, Kindt J H, Thompson J B, Del Amo Y, Stachelberger H, Brzezinski M A, Stucky G D, Morse D E and Hansma P K 2003 Atomic force microscopy study of living diatoms in ambient conditions *J. Microsc.—Oxf.* **212** 292–9

Gutsmann T, Hassenkam T, Cutroni J A and Hansma P K 2005 Sacrificial bonds in polymer brushes from rat tail tendon functioning as nanoscale velcro *Biophys. J.* **89** 536–42

Hansma P K, Fantner G E, Kindt J H, Thurner P J, Schitter G, Turner P J, Udwin S F and Finch M M 2005 Sacrificial bonds in the interfibrillar matrix of bone *J. Musculoskelet. Neuronal. Interact.* **5** 313–5

Hansma P K, Turner P J and Ruoff R S 2007 Optimized adhesives for strong, lightweight, damage-resistant, nanocomposite materials: new insights from natural materials *Nanotechnology* **18** 044026

Hassenkam T, Gutsmann T, Hansma P, Sagert J and Waite J H 2004 Giant bent-core mesogens in the thread forming process of marine mussels *Biomacromolecules* **5** 1351–5

Housner G W, Bergman L A, Caughey T K, Chassiakos A G, Claus R O, Masri S F, Skelton R E, Soong T T, Spencer B F and Yao J T P 1997 Structural control: past, present, and future *ASCE J. Eng. Mech.* **123** 897–971

Jackson A P, Vincent J F V and Turner R M 1988 The mechanical design of nacre *Proc. R. Soc.* B **234** 415–40

Kratky O and Porod G 1949 Rontgenuntersushung geloster fagenmolekule *Recl. Trav. Chim.* **68** 1106–23

Kuhn W and Grun F 1942 Relationships between elastic constants and stretching double refraction of highly elastic substances *Kolloidn. Zh.* **101** 248

Kwakernaak H and Sivan R 1972 *Linear Optimal Control Systems* (New York: Wiley–Interscience)

Schaffer T E *et al* 1997 Does abalone nacre form by heteroepitaxial nucleation or by growth through mineral bridges? *Chem. Mater.* **9** 1731–40

Scruggs J T and Iwan W D 2003 Control of a civil structure using an electric machine with semiactive capability *J. Struct. Eng.* **129** 951–9

Smith B L, Schaffer T E, Viani M, Thompson J B, Frederick N A, Kindt J, Belcher A, Stucky G D, Morse D E and Hansma P K 1999 Molecular mechanistic origin of the toughness of natural adhesives, fibres and composites *Nature* **399** 761–3

Soong T T and Costantinou M C 1994 *Passive and Active Structural Vibration Control in Civil Engineering* (New York: Springer)

Soong T T and Spencer B F 2002 Supplemental energy dissipation: state-of-the-art and state-of-the-practice *Eng. Struct.* **24** 243–59

Spencer B F Jr, Dyke S J and Deoskar H S 1998 Benchmark problems in structural control: part 1-active mass driver system *Earthq. Eng. Struct. Dyn.* **27** 1127–39

Spencer B F Jr, Dyke S J, Sain M K and Carlson J D 1997 Phenomenological model for magnetorheological dampers *J. Eng. Mech.* **123** 230–8

Spencer B F Jr and Nagarajaiah S 2003 State of the art of structural control *J. Struct. Eng.* **129** 845–56

Sun C, Fantner G E, Adams J, Hansma P K and Waite J H 2007 The role of calcium and magnesium in the concrete tubes of the sandcastle worm *Exp. Biol.* **210** 1481–8

Thompson J B, Kindt J H, Drake B, Hansma H G, Morse D E and Hansma P K 2001 Bone indentation recovery time correlates with bond reforming time *Nature* **414** 773–6

Thurner P J, Erickson B, Jungmann R, Schriock Z, Weaver J C, Fantner G E, Schitter G, Morse D E and Hansma P K 2007 High-speed photography of compressed human trabecular bone correlates whitening to microscopic damage *Eng. Fract. Mech.* **74** 1928–41

Thurner P J *et al* 2006 High-speed photography of the development of microdamage in trabecular bone during compression *J. Mater. Res.* **21** 1093–100

Zaremba C M, Belcher A M, Fritz M, Li Y L, Mann S, Hansma P K, Morse D E, Speck J S and Stucky G D 1996 Critical transitions in the biofabrication of abalone shells and flat pearls *Chem. Mater.* **8** 679–90